モデルに留置する多孔薄膜モデルとしては，実際にカバードステントが展開された時のカバー薄膜とほぼ同じ25μm の膜厚をもつポリイミドフィルムに，図 3 に示すように正方格子状に円型微細孔をエキシマレーザーによって搾孔することで多孔化した．なお，加工する微細孔の直径と開口率は，表 1 に示すように系統的に変化させた．なお，微細孔面積と多孔薄膜の開口率$\tilde{A}$の関係は，

$$\tilde{A} \equiv \frac{\pi d^2 / 4}{a^2} \tag{3}$$

で表わされる．ここで， dは微細孔直径，aは正方格子状に配置された微細孔のピッチ間距離である．

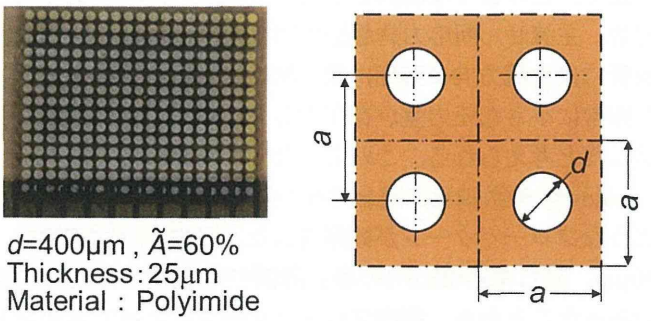

Fig. 3 Outline of cover film model with micro-pores fabricated by excimer laser.

Table 1 Dimensions of fabricated micro-pore.

d mm	100, 200, 300, 400, 500
$\tilde{A}$ %	23.6, 36, 48, 60

2・3 生体外模擬循環回路

生体外模擬実験用の循環回路の概略図を図 4 に示す．本回路は，タンクに貯められた模擬血液（45wt%グリセリン水溶液，密度ρ=1090kg/m^3，動粘度ν=4.0mm^2/s）を，遠心ポンプによって圧送し，バルブと流量計で流量を調整した後に，親血管モデルに流入させ，その後タンクに戻す閉ループ循環系とした．実験では，予め作動流体中に流れの可視化のための散乱粒子（二酸化ケイ素粉末，密度ρ=1950kg/m^3，平均粒径 d=20μm）を混入してあり，半導体レーザー（カトウ光研(株)：PIV Laser G1000-YK, 532nm CW, 1.0W））を光源とした厚さ 1mm のレーザーシートを照射することで， 動脈瘤モデル内流れを高輝度化し，側方に設置した高速度カメラ（(株)フォトロン：FastCam-Max 120KC, 1024×1024 pixel）で撮影した．得られた可視化画像を基に，動脈瘤内の流脈線画像の再構築や，相互相関法による PIV（Intelligent Laser Applications GmbH: VidPIV 4.0）によって速度ベクトルを求めた．

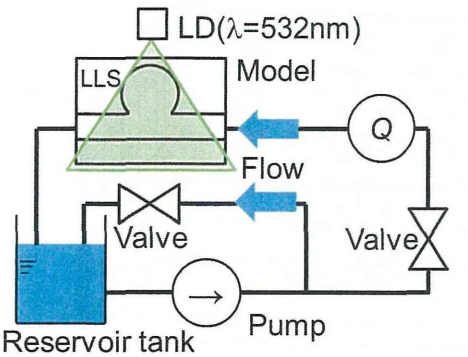

Fig. 4 Schematic diagram of cerebral blood flow simulator for in-vitro experiment.

3. 結果および考察

3・1 動脈瘤モデル内のフローパターン

可視化実験結果の一例として，親血管の Reynolds 数が Re=800 で多孔薄膜モデルを設置していない場合と微細孔径 d=400mm，開口率$\tilde{A}$=60%の多孔薄膜モデルを設置し Reynolds 数を Re=170~950 で変化させたときに可視化した瘤内ストロボ画像を図 5 に表す．なお可視化画像中で，親血管の流れは左から右方向である．この結果から，薄膜を留置しなかった場合や，留置しても流れの抑制効果が低い場合は，瘤内全域にわたる大きな旋回流[16]が観察された．これは，瘤ネック部付近の流体が親血管内流れによって生じる流れの粘性せん断に誘起されて流動し，これが瘤壁面に沿って流れることで大きな循環流となったキャビティーフローの一種と考えられる．この流れの旋回速度は非常に速く，このような流れを主流せん断応力誘起型旋回流とした．一方，非常に小さな開口の多孔薄膜を留置した場合，主流せん断応力誘起型旋回流とは逆回転で，非常にゆっくりとした半円状の旋回流れ[16]が観察できた．親血管には主流方向に壁面に働く粘性せん断応力による圧力損失が生じており，設置した多孔薄膜の各微細孔間でも非常に小さな圧力差が存在する．この圧力差が駆動力となり，非常にゆっくりとした円弧状の流れパターンを示したと考えられる．このような流れを摩擦圧力損失誘起型半旋回流とした．動脈瘤モデル内では，親血管の Reynolds 数や微細孔直径と薄膜の開口率の違いによっては，これら 2 つの間の遷移状態もしくは 2 つが共存するようなフローパターンが観察された．過去の動物実験で，カバードステントの留置効果が確認された孔直径 d=100μm．開口率$\tilde{A}$=23.6%の多孔薄膜[4-5]を留置したときに観察された瘤内フローパターンが，摩擦圧力損失誘起型であったことから，瘤内フローパターンによってステントの留置効果を定性的に予測できると考えられた．そこで，これらのフローパターンが発生する条件を開口率と孔直径，Reynolds 数でマッピングした結果を図 6 に示す．同じ多孔薄膜でも，Reynolds 数が変化すると瘤内流れが遷移する場合があることが分かった．また，例えば開口率が$\tilde{A}$=60%であっても微細孔径が d=100μm の場合は，Reynolds 数が変化しても発生したフローパターンは変わらなかったのに対して，d=500μm の場合は，3 つ全てのパターンが現れており，同じ開口率でも微細孔径が小さい方が，Reynolds 数の変化の影響を受けにくいことが分かった．

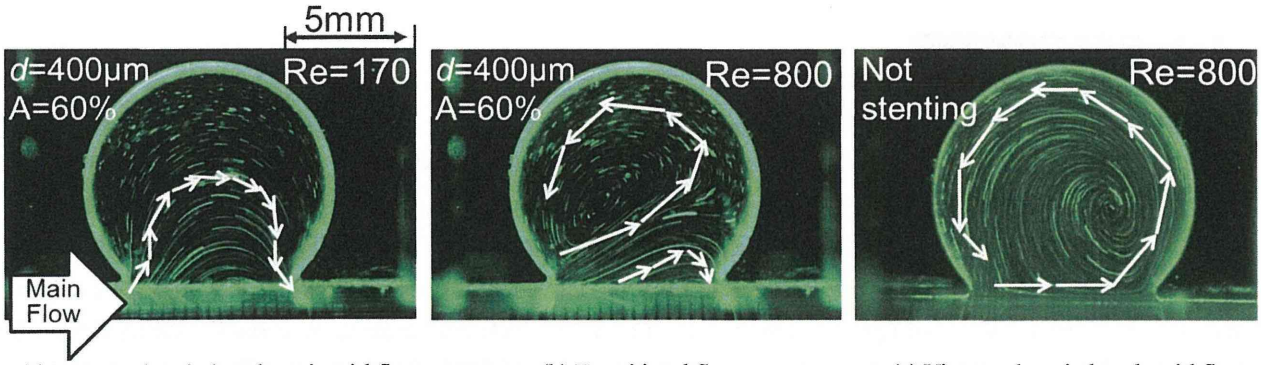

(a) Pressure loss induced semi-swirl flow (b) Transitional flow (c) Viscous shear induced swirl flow

Fig. 5 Typical visualized flow pattern in the aneurysm model.

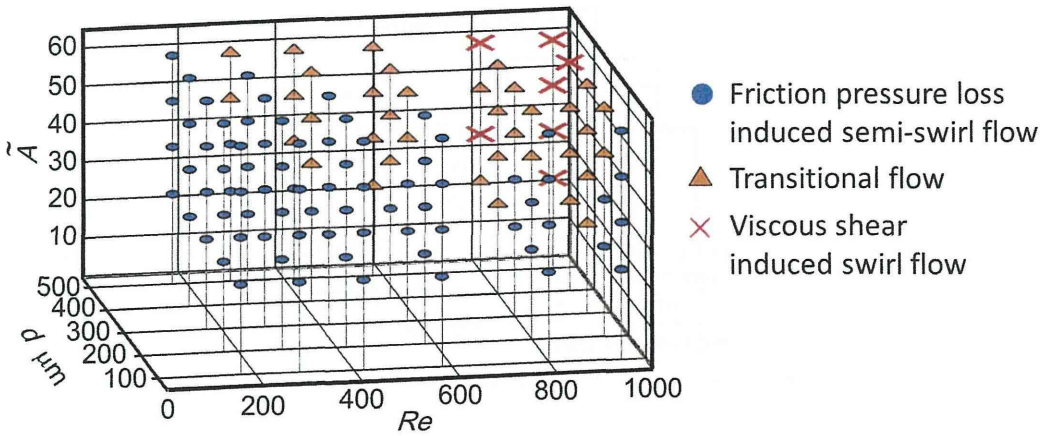

Fig. 6 Map of observed flow pattern.

3・2 ステント留置効果の定量評価

次に薄膜の留置効果の定量評価を試みた．カバードステントでは，動脈瘤ネック部に多孔薄膜を留置することで，親血管から瘤内に流入する血流を遮断もしくは抑制し，瘤内流れをよどませることで，血栓を形成し塞栓することを狙っている．このため，塞栓能の定量評価には，血流の血栓形成に関する指標が必要となるが，現時点で血栓形成について，一定のしきい値を与える物理パラメータはまだ無い．そこで本研究では，瘤内血流が停滞することによって，血液が凝固・血栓化するための判断指標として，以下の3つの力学的パラメータを求めた．

瘤内血流の運動エネルギー

特定の領域内の流動について，速度ベクトルの算術平均を計算することは，最も簡単な評価法であるが，瘤内流れのように回転流れの場合，逆流があると正しく評価できなくなる．また動脈瘤破裂の予測では，親血管部での血流の運動エネルギー損失が大きい場合，破裂に至るという報告があり[17]，動脈瘤が存在することによって，親血管の主流のエネルギー散逸が大きいほど，瘤破裂に至る可能性が高いと考えられていることから，本研究では瘤内の単位体積あたりの血流が有する運動エネルギーを求めた．

瘤内に現れた旋回流の循環

先に述べたように，動脈瘤内では旋回流が形成されており，多孔薄膜を留置することでその回転速度が遅くなっていたことから，その回転強さを表す指標として，瘤内の単位体積あたりの流れの循環を求めた．

瘤内血流の平均せん断速度

血液中の血栓形成には，血液のせん断変形が重要な力学的刺激であり，その振る舞いは高せん断速度領域と低せん断速度領域とで異なっていることが知られている[18]．本研究のように流れの停滞による血栓形成については，例えば遠心ポンプ型人工心臓の開発ではせん断速度が $300s^{-1}$ 以下になると血栓形成の危険性が高まる[19]と言われている．また，貝原らによる静脈血栓症発現機構に関する研究では，赤血球膜に存在するタンパク質であるエリスロエラスターゼ-IX (erythroelastase-IX, 以下 EE-IX) によって酵素による凝固第 IX 因子 (factor IX, 以下 F-IX) の活性化がトリガーとなって起こる血液凝固反応の存在が明らかにされており，EE-IX による F-IX の活性化は，せん断速度 $1s^{-1}$ 以下のオーダーで起きると報告されている[20-22]．そこで本研究では，血流停滞による血栓形成指標として，瘤内平均せん断速度を求めた．

具体的なデータ処理方法としては，可視化画像から瘤モデル内の速度分布を PIV により計測し，100 時刻の平均を取った動脈瘤内の速度ベクトル場から式(4)～(6)に従って，速度 V，せん断速度$\dot{\gamma}$，渦度ζの各分布を求めた．

$$V=\sqrt{u^2+v^2} \tag{4}$$

$$\dot{\gamma}=\frac{\partial v}{\partial x}+\frac{\partial u}{\partial y} \tag{5}$$

$$\zeta=\frac{\partial v}{\partial x}-\frac{\partial u}{\partial y} \tag{6}$$

なお実験は，過去の動物実験で動脈瘤の確実な塞栓が確認された開口率$\tilde{A}$=23.6%，孔径 d=100μm の薄膜と，先の流動様式の予測で最も大きい開口を有する開口率$\tilde{A}$=60%，孔径 d=100～500μm の薄膜に対して行った．

結果の一例として，図7に Re=800 における多孔薄膜留置前と開口率$\tilde{A}$=60%，孔径 d=500μm の薄膜を留置した瘤モデルの速度ベクトルと速度，せん断速度，渦度の各分布図を示す．この結果から，多孔薄膜留置前には，瘤ネック部で瘤内血液が駆動されるため，親血管下流側ネック部近傍で流れが瘤壁に沿って急速に曲げられており，局所的に高い速度，せん断速度，渦度を示した．一方，留置後は，これらの力学パラメータの分布は親血管上流側ネック部付近で最も大きな値を示したが，明らかにこれらの値が小さくなっていた．このように，力学パラメータの分布傾向と指示値が，多孔薄膜留置前後で大きく変わっていることから，瘤内フローパターンによって，ある程度多孔薄膜の留置効果を予測できると考えられるが，より定量的に留置効果を評価するために，式(7)～(9)に示す定義に基づいて，瘤内の単位体積辺りの平均運動エネルギー$\bar{K}$，平均せん断速度$\bar{\dot{\gamma}}$，循環$\bar{\Gamma}$を求めた．

$$\overline{K} = \frac{\int_{A_{an}} \frac{1}{2}\rho V^2 \, W dA}{\int_{A_{an}} W dA} = \frac{\int_{A_{an}} \frac{1}{2}\rho V^2 \, dA}{\int_{A_{an}} dA} \tag{7}$$

$$\overline{\dot{\gamma}} = \frac{\int_{A_{an}} |\dot{\gamma}| \, W dA}{\int_{A_{an}} W dA} = \frac{\int_{A_{an}} |\dot{\gamma}| \, dA}{\int_{A_{an}} dA} \tag{8}$$

$$\overline{\Gamma} = \overline{\zeta} = \frac{\int_{A_{an}} |\zeta| W \, dA}{\int_{A_{an}} W dA} = \frac{\int_{A_{an}} |\zeta| \, dA}{\int_{A_{an}} dA} \tag{9}$$

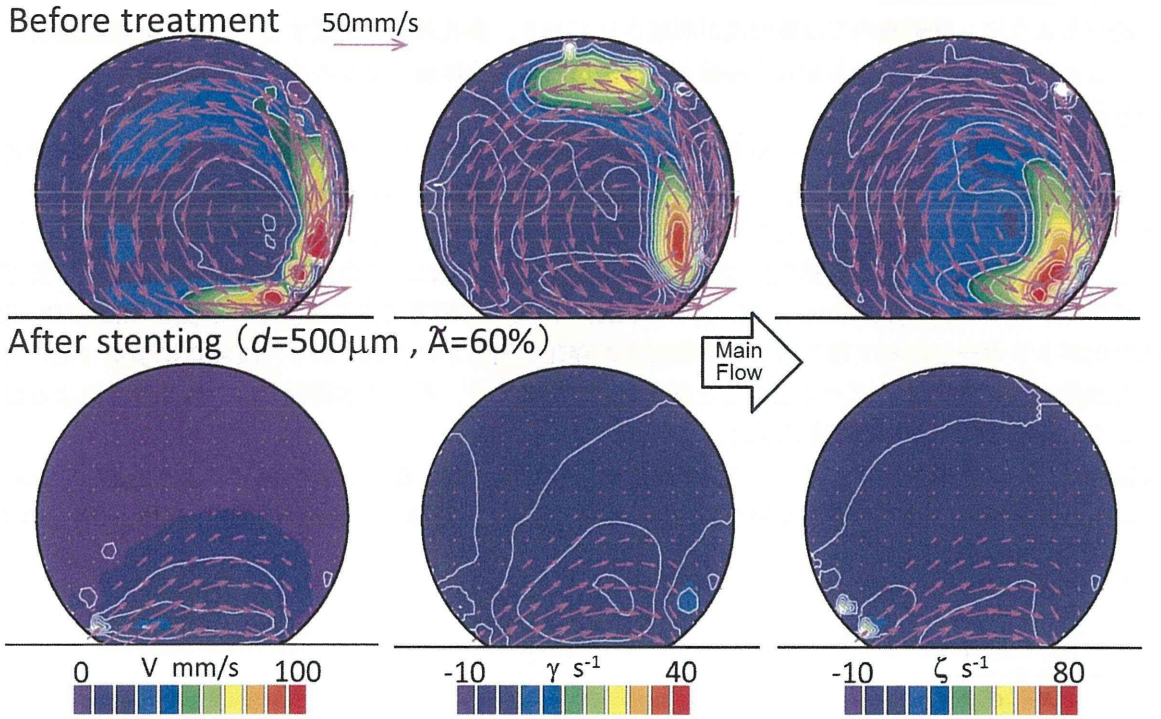

(a) Kinetic energy (b) Shear rate (c) Circulation

Fig. 7 Counter map of flow speed, shear rate and vorticity distribution in the aneurysm model with a micro-porous film.

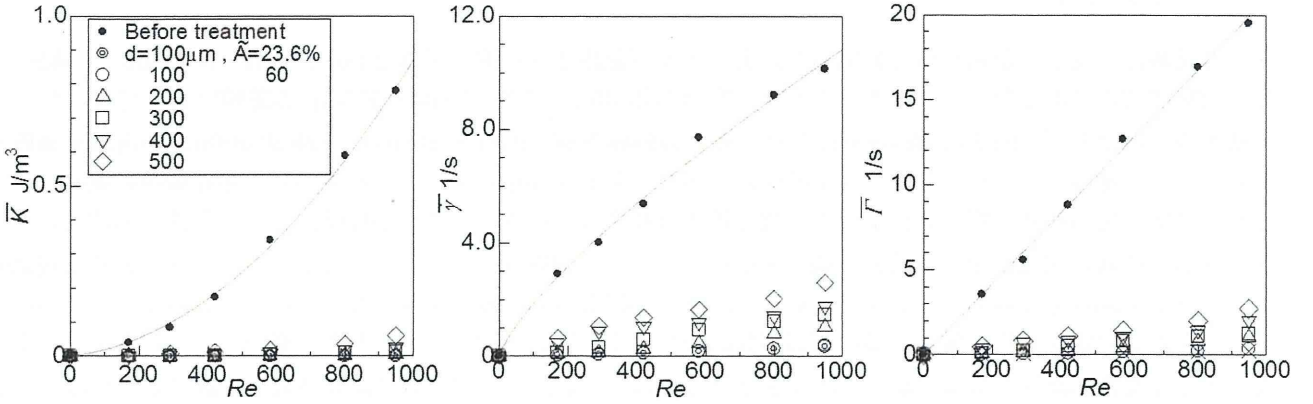

(a) Kinetic energy (b) Shear rate (c) Circulation

Fig. 8 Effect of micro-porous stent placement with volumetric mean kinetic energy, shear rate and circulation in aneurysm cavity.

これらの定義を基に各実験条件の力学パラメータを求めた結果を図 8 に示す．また，多孔薄膜留置の効果を考察するため，多孔薄膜の留置前後の比を取った結果を図 9 に示す．

その結果，孔径や開口率に関わらず薄膜の留置によって，これら力学量は大幅に抑制でき，薄膜留置前と比べ運動エネルギーが 7%以下，血栓形成指標であるせん断速度は 20%以下に抑制できた．特に孔径 100μm の薄膜については，過去の動物実験で瘤閉塞の治療効果が確認できていた開口率 23.6%よりも大きく開口させた開口率 60%の薄膜でも，その流れ抑制効果はほとんど変わらないことが分かった．ここで，貝原らによる静脈血栓形成に関するせん断速度の閾値 $1s^{-1}$[20]を，ステント留置後の塞栓可能な必要条件とすると，想定した Reynolds 数範囲では孔径 200μm 以下の微細孔であれば開口率 60%でも十分に瘤の塞栓が期待されることが示唆された．

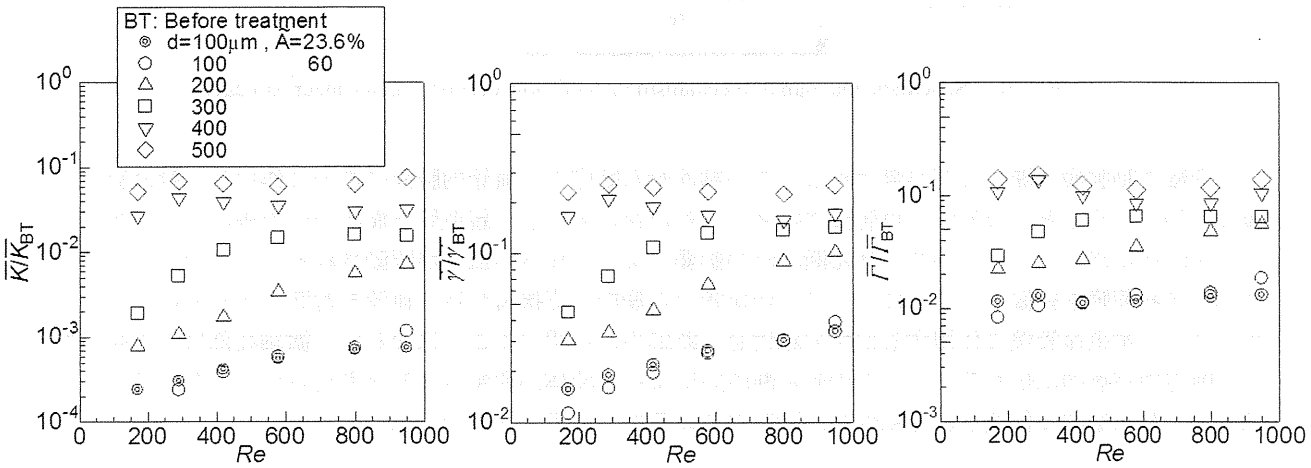

(a) Kinetic energy (b) Shear rate (c) Circulation

Fig. 9 Comparison of embolization indexes with before treatment and after stenting.

3・3 瘤内フローパターンと塞栓性能の予測

図 6 で示したように，開口率が同じにも関わらず，孔直径が異なると瘤内フローパターンが異なる場合があったこと，また図 5 で示したように多孔薄膜留置後は，微細孔の開孔を介して親血管の壁面に作用する壁ずり応力による粘性力が瘤内の血液を駆動していると考えられたことから，多孔薄膜を留置することによって瘤内の血液を駆動する力の大きさについて考察し，そこから瘤内流れの予測を試みた．

本実験での親血管流れの Reynolds 数は Re<2000 であることから，親血管の血流は十分に発達した層流であると仮定する．ここで，実験では親血管モデルの断面形状は正方形断面としているために，正方形断面の 1 辺の長さを直径とする円管と水力平均直径が同じであり，単位長さ当たりの圧力損失が等価であるため，断面形状の違いが流速分布などに及ぼす影響は無視する．図 10 に示すように親血管の管軸を通る縦断面における親血管内流速分布 u は，血管中心軸を原点とする半径外側方向への座標を y，管中心から血管壁までの距離を y_0(=D_h/2)，断面内平均流速を$\bar{U}$とすると Hagen–Poiseuille の式として式(10)で表される．

$$u = 2\bar{U}\left(1-\left(\frac{y}{y_0}\right)^2\right) = 2\bar{U}\left(1-\left(\frac{2y}{D_h}\right)^2\right) \tag{10}$$

親血管壁面における壁面せん断応力の大きさは，Newton の粘性法則から，壁面における速度勾配と粘性係数の積として式(11)と書くことができる．

$$\tau_w \equiv \left|\mu\frac{du}{dy}\right|_{y=y_0} = \frac{8\mu\bar{U}}{D_h} \tag{11}$$

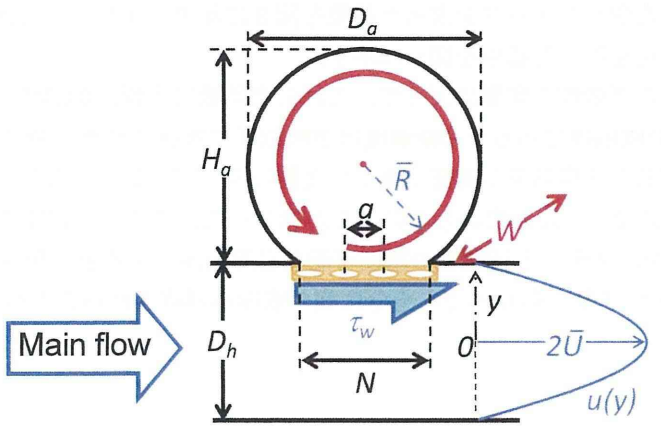

Fig. 10 Schematic diagram of mechanism of swirl flow occurring in an aneurysm cavity.

血管壁に動脈瘤の開口などが無ければ，この粘性せん断応力が血管内腔面に均一に作用し，親血管内での圧力損失と釣り合うことになるが，血管壁に瘤ネック部が存在すると，親血管と瘤内の圧力差によって血流が直接瘤内に流れ込んだり，ネック部でのせん断流れの影響によって瘤内の血液が駆動されることとなる．そこで瘤ネック部に多孔薄膜を留置することによって，親血管から瘤内に直接流れ込む血流を遮断できると仮定すると，薄膜表面には，本来血管壁に作用するはずの粘性せん断応力が作用することになるが，微細孔部はその開口を介してせん断応力が瘤内に伝わるため，このせん断応力によって流体が駆動されると考えられる．多孔薄膜の 1 つの微細孔当たりに瘤内に伝達される粘性せん断応力による力（以下，粘性力）は，

$$F_\tau = \tau_w A_p = \frac{\pi d^2}{4}\tau_w \tag{12}$$

となる．瘤ネック部には開口率$\tilde{A}$（開口ピッチ a）に応じて，親血管主流方向に n 個

$$n = \frac{N}{a} = \frac{N}{\sqrt{\dfrac{4\tilde{A}}{\pi d^2}}} \tag{13}$$

の微細孔が列ぶことになる．よって，親血管の血流が瘤ネック部を通過するときに，微細孔を介して伝わる瘤内の流体を駆動する粘性力は，親血管壁に作用する壁面せん断応力と微細孔の数に比例する．

$$F_{\mathrm{PV}} = nF_\tau = n\frac{\pi d^2}{4}\tau_w \tag{14}$$

実際には，この力によって瘤内の血液が旋回運動することから，その旋回半径を$\bar{R}$と置くと，旋回運動のために使われる駆動トルクは，

$$T_{\mathrm{PV}} = F_{\mathrm{PV}}\bar{R} = n\tau_w\frac{\pi d^2}{4}\bar{R} \tag{15}$$

と表すことができる．ここで本研究の動脈瘤モデルは奥行き Wの円柱形状であり，その内部を旋回する流体塊も旋回半径$\bar{R}$で旋回していると考えると，その慣性モーメント I_Aは，

$$I_{\mathrm{A}} = \rho\int r^2 dV = 2\rho\pi W\int_0^{\bar{R}} r^3 dr = \frac{1}{2}\rho\pi\bar{R}^4 W \tag{16}$$

で与えられる．瘤の内壁での粘性抵抗などによるエネルギー散逸を無視すると，角運動保存則より旋回流の角加速度αは，駆動力となる親血管血流によるトルクと旋回する流体塊の慣性モーメントの比で求めることができる．

$$\alpha = \frac{d\omega}{dt} \equiv \frac{T_{PV}}{I_A} = \frac{n}{2\rho W \overline{R}} \tau_w \frac{d^2}{\overline{R}^2} \tag{17}$$

動脈瘤内の血流の旋回半径は流動状態によって変わるが，ここでは瘤内全域で流体塊が旋回運動するせん断応力誘起型旋回流を仮定し，瘤最大深さ H_a と瘤最大直径 D_a の算術平均を動脈瘤内腔平均半径 $\overline{R}$

$$2\overline{R} = \frac{D_a + H_a}{2} = \frac{D_a}{2}\left(1 + \frac{H_a}{D_a}\right) = \frac{D_a}{2}\left(1 + \frac{H_a}{N}\frac{N}{D_a}\right) = \frac{D_a}{2}\left(1 + AR \cdot BF\right) \tag{18}$$

と定義し，これを旋回半径とすると，式(17)は次のように表すことができる．

$$\therefore \frac{T_{PV}}{I_A} = \frac{32n}{\rho W D_a \left(1 + AR \cdot BF\right)^3} \tau_w \frac{d^2}{D_a^2} \tag{19}$$

なお，ここで動脈瘤の赤道面直径とネック幅の比は，動脈瘤形状パラメータの一つである

$$BF = \frac{N}{D_a} \tag{20}$$

ボトルネック係数（Bottleneck factor）である．

ここでは，エネルギー散逸を無視したが，(19)式に示す粘性力による駆動トルクと瘤内血流の慣性モーメントの比が大きいほど，瘤内の旋回流が強いことを意味することから，この値を使って瘤内流動様式を整理した．

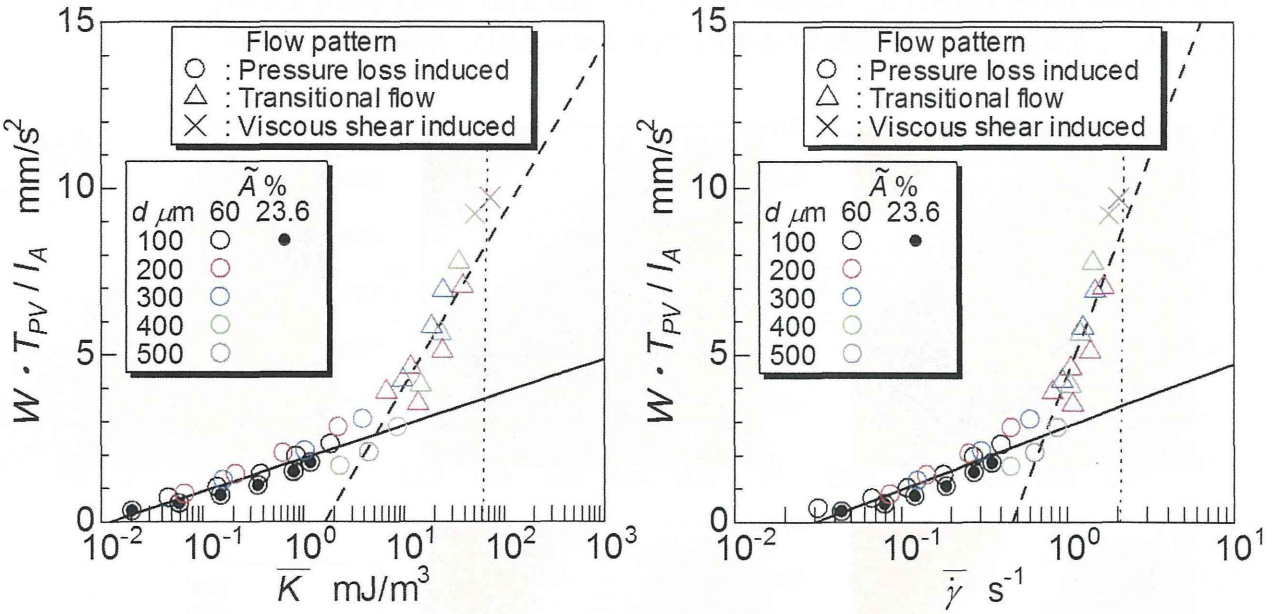

Fig. 11 Relationship between viscous shear force caused by shear flow in the vicinity of the parent vessel wall as the driving force of the aneurysm cavity flow and factor of embolization.

図 11 に本研究で提案する粘性力によるトルクと瘤内血流の慣性モーメントの比（親血管モデル単位奥行き：1mm 当たり）と瘤の塞栓指標として求めた瘤内平均運動エネルギーおよび平均せん断速度の関係を示す．なお図中において，各プロットは実際に観察された瘤内流れの流動パターンを，プロットの色は微細孔の開孔径を，さらに 3 本の直線は観察された 3 つの流動様式のプロットに対してそれぞれ最小二乗法によって得られた近似曲線を示している．なお，主流せん断応力誘起型旋回流のデータについては，運動エネルギーとせん断速度共に，非常に大きな値を示しており，ほぼ全てのデータがグラフの枠外にはみ出しているため，近似曲線がほぼ垂直に立っていることに注意されたい．この結果から，本研究で提案する粘性力によるトルクと瘤内血流の慣性モーメン

トの比は，流れの運動エネルギーと瘤内のせん断速度の増加に伴い，いずれも片対数グラフ上で単調に増加する傾向にあったが，流動パターンが変化するとその変化率が急激に変化することが分かった．このことは，瘤内の流れを駆動する親血管の粘性力と瘤内の流動状態が強い相関を示すことを意味しており，このことからも，今回提案した粘性力によるトルクと瘤内血流の慣性モーメントの比を使うことによって，多孔薄膜の留置効果を予測できると考えられる．また，先に述べた静脈性血栓症の発症の閾値となるせん断速度 $1s^{-1}$ に注目すると，摩擦圧力損失誘起型半旋回流ではこの閾値を超えることが無く，塞栓治療するためには圧力損失誘起型の流動にすることが必要であることが予測された．

次に，今回実験によって流動パターンを確認した多孔薄膜の孔直径と開口率，および親血管の Reynolds 数が，粘性力によるトルクと瘤内血流の慣性モーメントの比に及ぼす影響を求めた結果を図 12 に示す．これらの図は，動脈瘤ネック部に留置する多孔薄膜の開口率毎にグラフを描いており，横軸に親血管流れの Reynolds 数を，縦軸に微細孔直径を，カラーコンターが粘性力によるトルクと瘤内血流の慣性モーメントの比を，さらに図中のプロットが生体外模擬実験で観察された流動パターンを表している．

この結果から，粘性力によるトルクと瘤内血液の慣性モーメントの比は，親血管の Reynolds 数と多孔薄膜の孔直径と開口率が大きいほど高い値を示した．また，実際に観察された瘤内の流動パターンの境界線と粘性力によるトルクと瘤内血流の慣性モーメントの比の等高線のプロファイルは，開口率を固定すると孔直径と Reynolds 数を漸近線とする双曲線状であることが分かる．仮に各流動様式への遷移の閾値を $3.75mm/s^2$ および $8.75mm/s^2$ とすると，実際に観察された流動様式の境界とほぼ一致していた．過去に行った動物実験では，微細孔径が 100μm，開口率が 12.6%と 23.6%において，確実に動脈瘤を塞栓できていた[4-5]ことや，図 11 に示したように本指標と瘤内のせん断速度の関係が線形関係にあったことから，本指標を元にすることで，塞栓性能が予測できる可能性がある．ただし実際の脳動脈瘤では，親血管は曲がりを有する 3 次元形状であることから，その血流動態も 2 次流れを伴う複雑なものと予想される．本研究のモデルでは，親血管壁に作用する粘性せん断応力だけを考慮していることから，2 次流れに伴い直接瘤内に入る流れに対する抑止効果は，別途予測する必要がある．

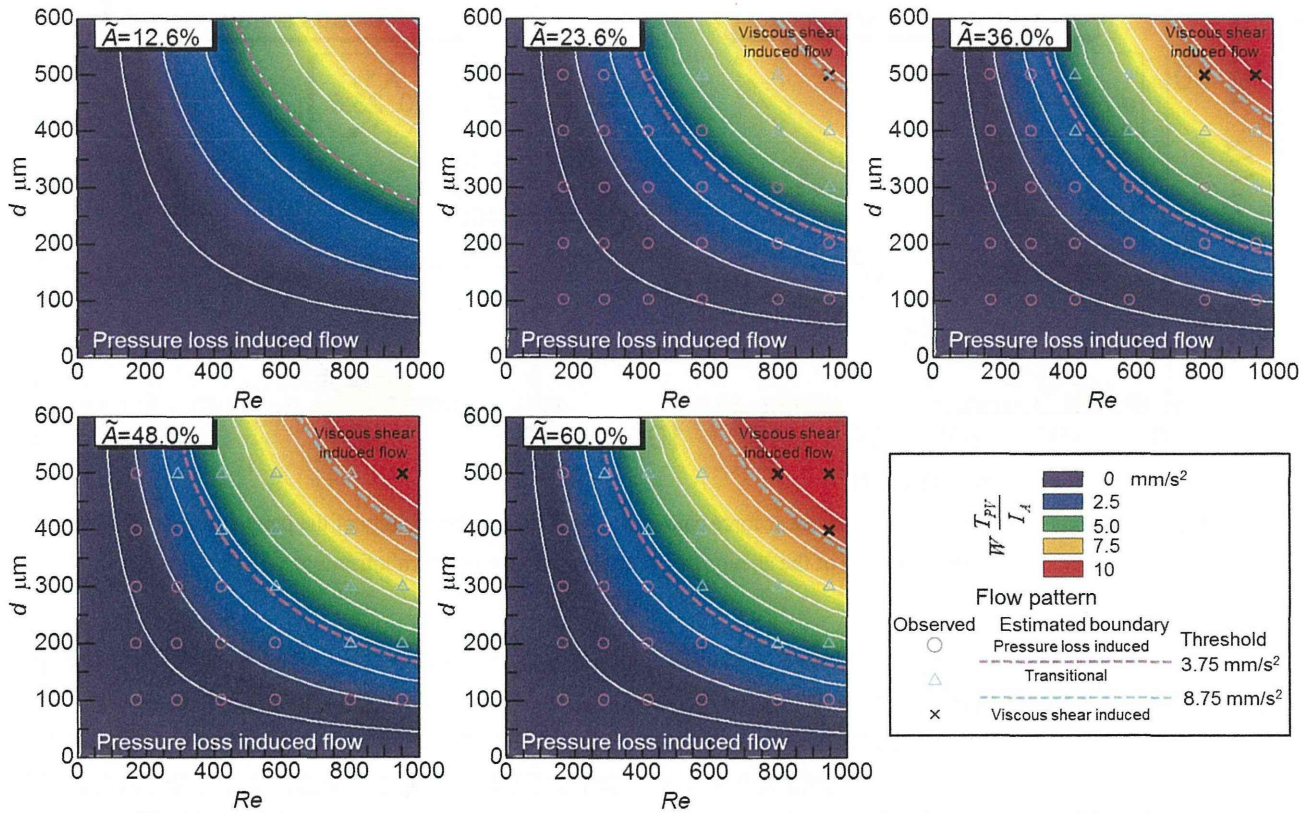

Fig. 12　Relationship between observed flow pattern in the aneurysm model and counter map of the ratio of the viscous shear force to rotational moment of the blood.

以上のことから，多孔薄膜を瘤ネック部に留置することで動脈瘤の塞栓を行う場合は，今回想定した Re<1000 の親血管においては，開口率$\tilde{A}$=60%の薄膜で，塞栓が期待できる孔直径は 100μm 以下，Re<700 では 200μm 以下であることが示唆された．また，駆動力の算出から予測された流動様式では，瘤が小さいほど旋回流が速くなることが示唆された．これは，小さな動脈瘤に対しては，大きな瘤と比べてステント留置効果が低減することを意味しており，個々の動脈瘤の形状パラメータを元に最適な微細孔を持つステントを選択する必要性が示唆された．今後，動物実験によってこれらの塞栓効果や動脈瘤の大きさが塞栓能に及ぼす影響について確認する予定である．また実際の脳動脈瘤では，親血管の血流は十分に発達した軸対称放物面状の速度分布では無く，親血管の曲がりや分岐の影響による 2 次流れ成分を有しており，その影響で親血管から直接瘤内に血流が入り込むことが予想され，今回の実験や論理モデルのような完全な嚢状型の動脈瘤よりも，より血流を停滞させにくいと考えられることから，その影響を考慮した実験および瘤内流れの予測が今後必要である．

4. 結　　語

嚢状動脈瘤の 2 次元モデルを使用した生体外模擬実験によって，カバードステントの多孔薄膜の塞栓性能の定量評価を行ったところ，薄膜留置によって瘤内流れを大幅に抑制できることが確認できた．また，従来と比べ約 2.5 倍の開口率を持つ開口率 60%の多孔薄膜についても，孔径を 300μm 以下にすることで，薄膜留置前と比べ瘤内流れの運動エネルギーを 1/100 以下，血栓形成指標であるせん断速度を 1/10 以下に抑制できた．また，同じ開口率でも，微細孔径が小さい方が，流れの抑制効果が大きく，親血管の Reynolds 数が変化しても，瘤内の流動様式が変化しにくいことが分かった．さらに，親血管内の血流によって発生する粘性力によるトルクが，動脈瘤内の血液を駆動していると仮定し，駆動トルクと動脈瘤内の血流の慣性モーメントの比を求めた結果，この値の大きさによって実際に観察された瘤内の流動パターンや瘤内の流れの運動エネルギーやせん断速度の比と相関があり，この値をつかって流動様式を予測できる可能性があることが分かった．この結果を使うと，動脈瘤の塞栓を期待できる孔直径は，開口率が 60%の場合，Reynolds 数が 1,000 以下の親血管においては 100μm 以下，Reynolds 数が 700 以下においては 200μm 以下であることが示唆された．また，動脈瘤の大きさや形によって，動脈瘤を塞栓可能な多孔薄膜形状が異なる可能性があり，これらの影響について考慮した設計指標の確立が必要と考えられる．

謝　　辞

本研究の一部は，厚生労働省　科学研究費補助金（23－実用化（臨床）－指定－003），日本学術振興会　科学研究費補助金（19700390），平成 24 年度　関西大学大学院理工学研究科　高度化推進研究費，関西大学先端科学技術推進機構　平成 24～26 年度「流体・弾性膜連成現象研究グループ」研究費によって行われた．

文　　献

(1) Nakayama Y., Nishi S., Ueda-Ishibashi H. and Matsuda T., “Fabrication of micropored elastomeric film-covered stents and acute-phase performance“, *Journal of Biomedical Materials Research. Part A*, Vol. 64, No.1, (2003), pp.52-61.

(2) Nishi S., Nakayama Y., Ueda-Ishibashi H. and Matsuda T., “Embolization of experimental aneurysms using a heparin-loaded stent graft with micropores”, *Cardiovascular Radiation Medicine*, Vol. 4, No. 1, (2003), pp.29–33.

(3) Nakayama Y., Nishi S., Ueda-Ishibashi H. and Matsuda T, “Surface microarchitectural design in biomedical applications : In vivo analysis of tissue ingrowth in excimer laser-directed micropored scaffold for cardiovascular tissue engineering”, *Journal of Biomedical Materials Research*, Vol. 51, No. 3, (2000), pp.520–528.

(4) Nishi S., Nakayama Y., Ishibashi-Ueda H., Okamoto Y. and Kinoshita Y., “High-performance self-expanding stent graft: development and application to experimental aneurysms”, *Journal of Artificial Organs*, Vol. 12, No. 1, (2009) pp.35–39.

(5) Nishi S., Nakayama Y., Ishibashi-Ueda H., Okamoto Y. and Yoshida M., “Development of microporous self-expanding stent grafts for treating cerebral aneurysms: designing micropores to control intimal hyperplasia”, *Journal of Artificial Organs*, Vol. 14, No. 4, (2011), pp.348–356.

(6) Ku J. P., Elkins, C. J. and Taylor C. A., "Comparison of CFD and MRI flow and velocities in an in vitro large artery bypass graft model", *Annals of Biomedical Engineering*, Vol. 33, No. 3, (2005), pp. 257–269.

(7) Imai Y., Sato K., Ishikawa T. and Yamaguchi T. "Inflow into saccular cerebral aneurysms at arterial bends", *Annals of Biomedical Engineering*, Vol. 36, No. 9, (2008), pp. 1489-1495.

(8) Zhao M., Amin-Hanjani S., Ruland S., Curcio A. P., Ostergren L. and Charbel F. T., "Regional cerebral blood flow using quantitative MR angiography", *American Journal of Neuroradiology*, Vol. 28, No. 8, (2007), pp. 1470-1473.

(9) 中西助次, 松尾秀信, “二次元流路内の脈動流”, 広島工業大学研究紀要, Vol. 29, (1995), pp. 67–73.

(10) Ujiie H., Tachibana H., Hiramatsu O., Hazel A. L., Matsumoto T., Ogasawara Y., Nakajima H., Hori T., Takakura K. and Kajiya F., "Effects of size and shape (aspect ratio) on the hemodynamics of saccular aneurysms: a possible index for surgical treatment of intracranial aneurysms", *Neurosurgery*, Vol. 45, No. 1, (1999), pp. 119–130.

(11) Ujiie H., Tamano Y., Sasaki K. and Hori T., "Is the aspect ratio a reliable index for predicting the rupture of a saccular aneurysm?", *Neurosurgery*, Vol. 48, No. 3, (2001), pp. 495–503.

(12) Weir B., Amidei C., Kongable G., Findlay J. M., Kassell N. F., Kelly J., Dai L. and Karrison T. G., "The aspect ratio (dome/neck) of ruptured and unruptured aneurysms", *Journal of Neurosurgery*, Vol. 99, No. 3, (2003), pp. 447-451.

(13) Nakayama Y., Nishi S. and Ishibashi-Ueda H., "Fabrication of drug-eluting covered stents with micropores and differential coating of heparin and FK506", *Cardiovascular Radiation Medicine*, Vol. 4, No. 2, (2003), pp.77-82.

(14) Sato S., Nakayama Y., Miura Y., Okamoto Y., Asano H., Ishibashi-Ueda H., Zhou Y. M., Hayashida K., Matsuhashi T., Seiji K., Sato A., Yamada T., Takahashi S. and Ishibashi T., "Development of self-expandable covered stents", *Journal of Biomedical Materials Research Part B: Applied Biomaterials*, Vol. 83, No. 2, (2007), pp. 345–353.

(15) Sato S., Nakayama Y., Matsuhashi T., Seiji K., Matsunaga K., Takasawa C., Ishibashi T., Zhou Y. M., Ishibashi-Ueda H., Okamoto Y., Asano H. and Takahashi S., "Evaluation of self-expandable, FK506-coated, covered stents in canine animal model", *Journal of Biomedical Materials Research Part B: Applied Biomaterials*, Vol. 90, No. 2, (2009), pp. 647-652.

(16) Lieber B. B., Livescu V., Hopkins L. N. and Wakhloo A. K., "Particle image velocimetry assessment of stent design influence on intra-aneurysmal flow", *Annals of Biomedical Engineering*, Vol. 30, No. 6, (2002), pp. 768-777.

(17) 杉本充彦, “血栓形成過程：オーバービュー”, 脈管学, Vol. 51, No. 3, (2011), pp. 275-282.

(18) Qian Y., Takao H., Umezu M. and Murayama Y., "Risk analysis of unruptured aneurysms using computational fluid dynamics technology: preliminary results", *American Journal of Neuroradiology*, Vol. 32, No. 10, (2011), pp. 1948-1955.

(19) Yamane T., Maruyama O., Nishida M., Toyoda M., Tsutsui T., Jikuya T., Shigeta O. and Sankai Y., "The most profitable use of flow visualization in the elimination of thrombus from a monopivot magnetic suspension blood pump", *Artificial Organs*, Vol. 28, No. 4, (2004), pp.390–397.

(20) 貝原真, 岩田宏紀, 姫野龍太郎, “静脈血栓症発現機構に関する実験シミュレーション研究”, 理研シンポジウム 生体力学シミュレーション研究　プロジェクト第一期成果報告会　予稿集, (2004), pp. 70-80.

(21) 貝原真, “血栓形成と血液の流動—静脈血栓を中心に—”, 日本バイオレオロジー学会誌（B&R）, Vol. 18, No. 3, (2004), pp. 82-90.

(22) Kaibara M., "Rheological study on coagulation of blood with special reference to the triggering mechanism of venous thrombus formation", *Journal of Biorheology*, Vol. 23, No. 1, (2009), pp. 2–10.

Society For Biomaterials

Acceleration of robust "biotube" vascular graft fabrication by in-body tissue architecture technology using a novel eosin Y-releasing mold

Yasuhide Nakayama, Takahiro Tsujinaka

Division of Medical Engineering and Materials, National Cerebral and Cardiovascular Center Research Institute, 5-7-1 Fujishiro-dai, Suita, Osaka 565-8565, Japan

Received 25 June 2012; revised 28 March 2013; accepted 6 June 2013
Published online 2 August 2013 in Wiley Online Library (wileyonlinelibrary.com). DOI: 10.1002/jbm.b.32999

Abstract: A novel eosin Y-releasing mold was designed to accelerate the fabrication of *in vivo* tissue engineered autologous vascular prosthetic tissues, called the "biotubes." The mold was prepared by addition of an aqueous solution of eosin Y (1~6 w/v%) to the agar gel (0.3%), which was attached to the luminal surface of the microporous acrylate tube (diameter, 5 mm; length, 28 mm; pore size, 0.5 mmϕ). The eosin Y release period was controlled by the number of pores (3~160). On embedding the molds into dorsal, subcutaneous pouches of rats for 1 week, completely encapsulated biotubes, mainly consisting of collagen, with thick walls (418.2 ± 173.4 μm) and robust mechanical properties (elastic modulus, 956.2 ± 196.5 kPa; burst pressure 5850 ± 2383 mmHg) were formed. These values were, respectively, more than 4.3, 3.8, and 5.6 times greater than the corresponding controls (acrylate rods). The high elastic modulus of the biotubes was obtained even with a small number of micropores (3), and a low concentration of eosin Y (1%) within a very short embedding period (5 days), irrespective of rat weights. This innovative method for rapid production of vascular grafts with thick walls and robust mechanical properties may be adaptable for the sub-emergency clinical use of biotubes in regenerative medicine. © 2013 Wiley Periodicals, Inc. J Biomed Mater Res Part B: Appl Biomater, 102B: 231–238, 2014.

Key Words: eosin Y, biotube, vascular grafts, tissue formation, *in vivo* tissue engineering

How to cite this article: Nakayama Y, Tsujinaka T. 2014. Acceleration of robust "biotube" vascular graft fabrication by in-body tissue architecture technology using a novel eosin Y-releasing mold. J Biomed Mater Res Part B 2014;102B:231–238.

INTRODUCTION

Conventional grafts, such as Dacron or expanded polytetrafluoroethylene (ePTFE), have shown clinically satisfactory durability; however, they have several disadvantages, such as thrombogenicity; late stenosis and occlusion from intimal hyperplasia especially in small caliber grafts; susceptibility to infection; and lack of growth potential. The ongoing search for the ideal graft has sought to overcome these limitations through the development of various tissue-engineered vascular grafts and the reporting of their clinical utility. In such grafts, biodegradable polymers[1–3] or decellularized biomaterials[4,5] are commonly used as scaffolds to enable host cells to rebuild the vessel architecture; autologous cell seeding and culturing within bioreactors before *in vivo* placement is usually necessary to improve their antithrombogenicity and performance.

In an alternative approach, autologous tubular tissues, called biotubes, were developed through the application of *in-body* tissue architecture technology. These structures were evaluated for use as small-caliber vascular grafts (diameter, 1.5~3 mm) in animal experiments, where the biotubes were demonstrated to be able to withstand aortic pressures (burst pressure, ~1000 mmHg).[6] This technology is advantageous because the prostheses do not induce immunological rejection, exhibit nontoxic biocompatibility, and might adapt to the recipient's growth. In addition, these tissue prostheses can be fabricated in a wide range of shapes and sizes to suit each individual recipient. Most importantly, neither complex *in vitro* cell management nor special aseptic laboratory facilities are required, which are both expensive and time consuming.

Recently, this technology was applied to the development of heart valve tissues, with or without stents for transcatheter valve implantation. However, the wall thickness of the biotubes formed within the subcutaneous space was less than 100 μm, even after several months of embedding using the classical preparation molds.[7] The wall thickness of the biotubes was found to be somewhat controlled by the type and surface chemistry of the materials used in the molds. Previously, in order to accelerate the fabrication of biotubes, novel, wing-attached rod molds were designed for the tissue rolling process.[8] By using such molds, wall structures with functions similar to those of native arteries were acquired within 4 weeks, even though a 2-step *in vivo* tissue incubation process was required. In an alternative method, a novel drug-coated mold was designed using nicotine as a

Correspondence to: Y. Nakayama (e-mail: nakayama.yasuhide.ri@mail.ncvc.go.jp)
Contract grant sponsor: Grant-in-Aid for Scientific Research from the Ministry of Education, Culture, Sports, Science and Technology of Japan

model drug[9] due to its physiological angiogenic activity.[10] Nicotine was applied to the mold surface in a thin gelatinous matrix, using a photocurable gelatin, and tissue formation and rich angiogenesis in the biotubes were accelerated. After having embedded the nicotine-coated biotubes for 2 weeks, burst strengths of about 2700 mmHg were obtained.

The *in-body* tissue architecture technology is depend on tissue capsulation phenomenon, which is one of normal body defense mechanisms, induced by trivial stimulation such as very weak inflammation reaction against the material surface. Therefore, we estimated that the release of chemicals with little positive physiological activity also might have potential of acceleration of biotube preparation. According to the strategy esion Y was selected as a model chemical. There is little report on eosin Y about the physiological activity of tissue formation or anigiogenesis. Our urgent goal on the biotube development is shortening of preparation period of biotubes with thick and strong tissue walls in less than 1 week, suitable for sub-emergency cases.

MATERIALS AND METHODS

Preparation of an Eosin Y-eluting Mold

Eosin Y-eluting molds were prepared, according to the schematic diagram shown in Figure 1, using 3 kinds of acrylate parts, including a tube (outer diameter, 5 mm; wall thickness, 0.5 mm; length, 24 mm) with micropores (diameter, 0.5 mm; number of pores, 3–160 per mold, 0 for control), a rod (diameter, 2 mm; length, 24 mm), and 2 caps (diameter, 5 mm; length, 4 mm). The various acrylate parts were prepared using a three-dimensional inkjet printing system (Projet HD3000, 3D Systems, SC). A cap was connected to one end of the acrylate rod and the rod was inserted into the center of the lumen of the microporous acrylate tube (Figure 1, step 1). The aperture space between the tube and the rod was filled with agar (0.3%) (Figure 1, step 2). After room-temperature gelation of the agar, the rod was removed (Figure 1, step 3). The cylindrical space formed at the center of the agar gel was filled with a phosphate buffered saline (PBS) solution containing eosin Y (Figure 2, concentration, 0.5–6%, 0% for contol, Wako Pure Chemicals, Osaka, Japan), and the other end of the tube was capped (Figure 1, step 4). As a control, an acrylate rod, without micropores or eosin Y was used.

Biotube preparation

The acrylate molds, with or without eosin Y, were surgically embedded into dorsal, subcutaneous pouches of anesthetized Wistar rats ($n = 40$; weight range of 100–300 g). In each rat, four rods from the same group were embedded (at least $n = 6$ for each point in Figure 5). Anesthesia was induced by isoflurane (Nissan Chemical Industries, Tokyo, Japan; concentration, 1.5%, in oxygen; flow, 500 mL/min). After predetermined periods, 3 days to 2 weeks, the molds were harvested, with the surrounding capsular tissues, to obtain the biotubes.

All animal experiments were acute experiments performed under aseptic conditions in compliance with the *Guide for the Care and Use of Laboratory Animal*, published by the US National Institutes of Health (NIH Publication No 88-23, revised 1996). The research protocol (No. 12002) was approved by the ethics committee of the National Cardiovascular Center Research Institute (Osaka, Japan).

Measurement of eosin Y release

The amount of eosin Y released from the microporous molds was determined spectrophotometrically. After immersing the acrylate molds into a saline solution (100 mL), absorbance of the solution was measured at predetermined times, using a UV/visible light spectrophotometer (UV-1700, Shimadzu, Kyoto, Japan) at a wavelength of 518 nm.

Histological examination

Recovered biotube specimens were fixed in a 10% formalin solution and embedded in paraffin. For histological evaluations, the embedded tissue was thin-sectioned (3–5 μm) for routine hematoxylin and eosin staining. Some histological sections were stained with either Masson's trichrome stain for collagen or with elastica-van Gieson stain for elastin.

Measurement of elastic modulus

The elastic modulus of the biotubes was examined using a custom designed tensile tester. Tubular samples were cut circumferentially and opened. Tissue specimens, 10 mm × 10 mm, were tested under humid conditions. The load was recorded until the samples ruptured, with a tissue-extension rate of 0.05 mm/s. Elastic modulus values were obtained from the maximum slope of the deformation-force relationships.

Statistics

Results were expressed as the means of at least six tests and the standard errors of the mean were also calculated.

RESULTS

Release character of eosin Y

The water solubility of Eosin Y allowed it to easily penetrate the highly water-swelled agar gel, coloring the internal volume of the acrylate tube red (A and B in Figure 1). In the absence of the acrylate tube, an initial burst release of eosin Y occurred upon immersion of the colored agar into a PBS solution (Figure 3A); the microporous tube covering the gel restricted the release of the dye. Irrespective of the number of micropores in the tube, eosin Y was released almost linearly up to about 50% of the initial dye content (Figure 3A). The release rate, determined by the initial slope of the release curve, increased as the number of micropores increased (Figure 3B). The period over which the release of the dye occurred could be controlled by the number of micropores: the higher the number of micropores, the shorter the length of the estimated release period (Figure 3C).

Preparation of biotubes

When the acrylate molds, as controls, were embedded into the subcutaneous pouches of rats for 1 week, the molds

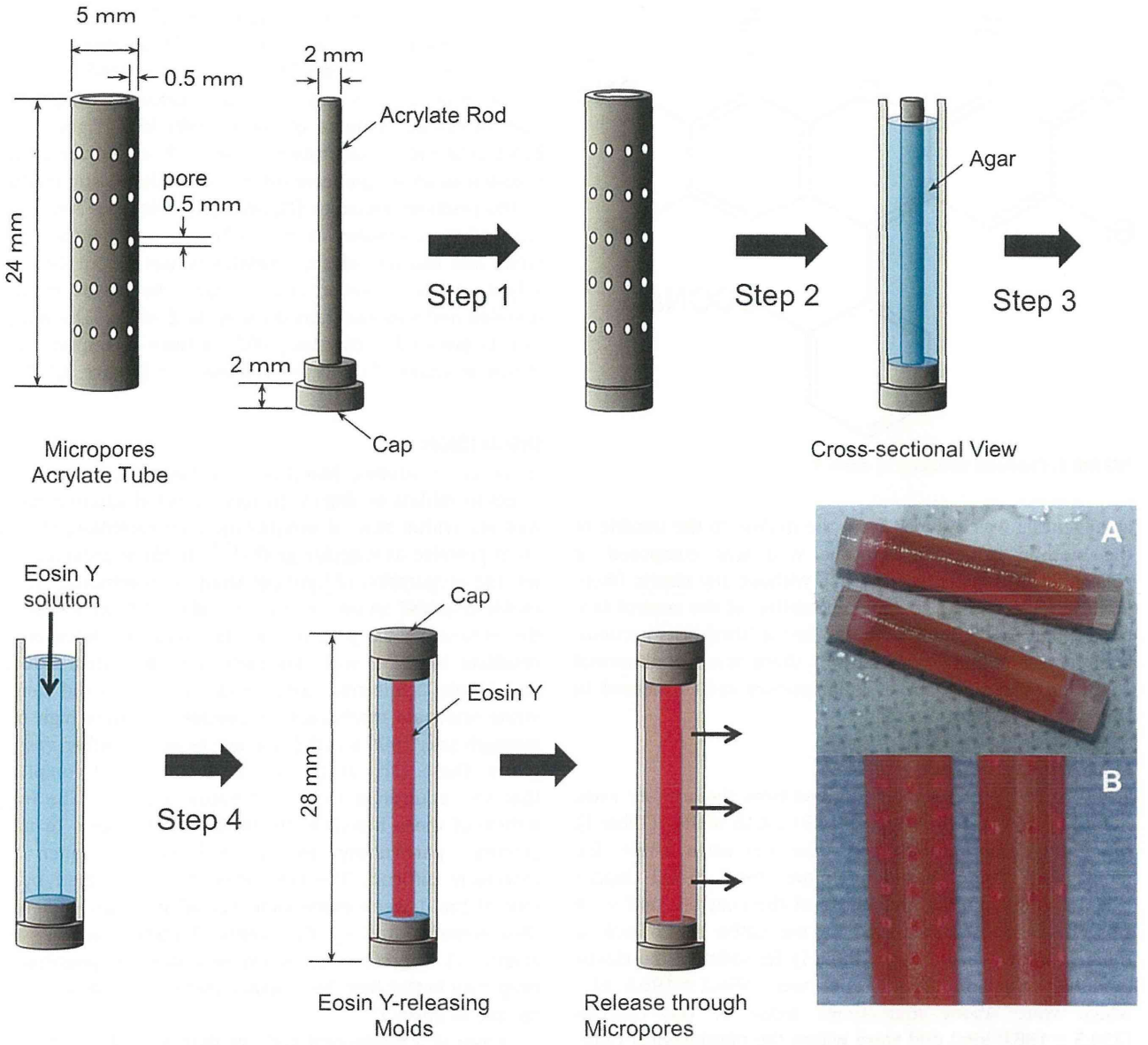

FIGURE 1. The sequential preparation method of eosin Y-releasing molds. A PBS solution of eosin Y was added to the agar tube (step 3), which was closely attached to the luminal surface of microporous acrylate tubes (step 2). Eosin Y was released through the micropores. The whole view (A) and the magnification view (B) of the eosin Y-releasing molds with micropores. [Color figure can be viewed in the online issue, which is available at wileyonlinelibrary.com.]

were covered with a very thin and almost transparent layer of connective tissue, similar to that observed in a previous report in which silicone molds were used as controls[11] [Figure 4(A)]. Because the developed tissues were fragile, complete harvesting of the molds was extremely difficult [Figure 4(B)]. On removal of the molds, the incomplete tubular connective tissues, with thin-walled membranes, collapsed [Figure 4(C)]. As indicated by the yellow arrows in Figure 4(G), the resultant biotubes had a thin wall thickness of $97.2 \pm 22.8\,\mu m$ (Table I), and demonstrated little vascular ingrowth into the biotube membrane.

In contrast, when the eosin Y-containing molds were embedded into the subcutaneous pouches of rats for 1 week, the area surrounding the molds was fully covered with thick connective tissue [Figure 4(D)]. The developed tissues were easily harvested from each subcutaneous pouch since there was little adhesion between the developed connective tissue and the surrounding original tissues [Figure 4(E)]. Upon removing the molds, tubular biotube tissues were obtained [Figure 4(F)]. Almost all of eosin Y (over 80%) was excluded from the mold after 1 week of embedding, irrespective of number of micropores. As indicated by the yellow arrow in Figure 4(J), the biotubes obtained were very thick-walled ($418.2 \pm 173.4\,\mu m$ in Table I) and intensely colored red, which was different from the color of eosin Y [Figure 4(F)]. Since tubular shape was maintained in the biotubes, their handling was very easy. As indicated by the yellow arrow heads in Figure 4(K), rich

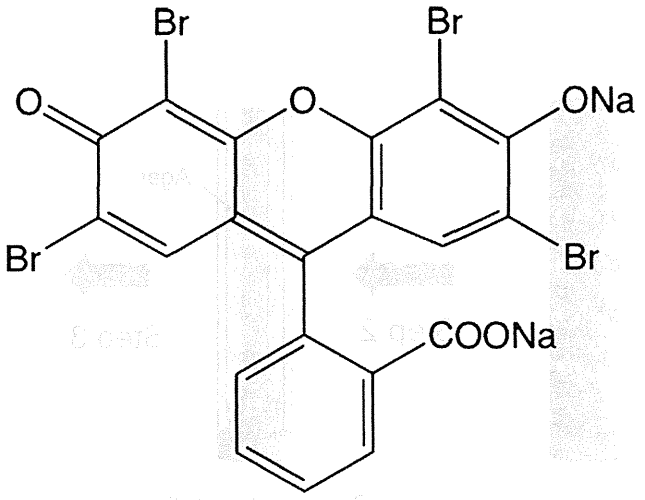

FIGURE 2. Chemical structure of eosin Y.

angiogenesis was induced from the middle to the outside of the biotube layer. The biotube wall was composed of collagen-rich tissue [Figure 4(K)], without any elastic fibers [Figure 4(L)], similar to the composition of the control biotubes [Figure 4(H,J)]. A large number of fibroblasts accumulated at the luminal surface, but there was no abnormal collection or infiltration of inflammatory cells observed in the walls of the biotubes.

Mechanical properties

The control biotube tissues, derived from the acrylate rods, burst at a luminal pressure of 1050 ± 446 mmHg (Table I). In contrast, biotubes formed from the eosin Y-releasing molds had burst strengths more than 5-fold higher (5850 ± 2383 mmHg) than those of the controls, and were close to the values measured for the native aortic arch or thoracic aorta (beagle dog) (Table I). In addition, the elastic modulus values of the biotubes were 956.2 ± 196.5 kPa, which were about four times those of the controls (254.5 ± 188.0 kPa) and were within the physiological range of values determined for aortic arches (499.4 ± 88.8 kPa) and aortas (1267.1 ± 353.3 kPa).

Biotubes with high elastic modulus values were obtained from the molds even with the smallest number of micropores (number of pores: 3), but only increased slightly as the number of pores was increased; biotubes with 80 pores had an elastic modulus of about 1000 kPa [Figure 5(A)]. Increasing the concentration of eosin Y in the molds also resulted in an insignificant difference in the elastic modulus of the resultant biotubes [Figure 5(B)]. Biotubes removed 3 days after placement in the subcutaneous pouches were weak and had low elastic modulus values (about 400 kPa) [Figure 5(C)]. However, after 5 days, the elastic modulus doubled and was maintained for up to 2 weeks. The weights of rats involved in the study did not have an impact on the elastic modulus of the recovered biotubes [Figure 5(D)].

DISCUSSION

In previous studies, biotubes have been used as vascular grafts in rabbits or dogs with reconstructed vascular tissues forming within several months after implantation, showing great promise as vascular grafts.[12,13] In these previous studies, the preparation of biotubes from the traditional, silicone molds required an embedding period of at least 1 month in the subcutaneous pouches of the animals. However, the resultant biotubes had extremely thin (less than 100 μm) and fragile connective tissue walls. The walls did demonstrate adequate mechanical properties, including high burst strength (ca., 1000 mmHg), for use as small caliber vascular grafts. These early biotubes also demonstrated compliance that was equivalent to that of native arteries.[7] The fragile nature of these biotubes meant that anastomosis to native arteries, particularly in an end-to-end manner, was extremely difficult. The connective tissues formed by the end of the 1-week embedding period were incomplete, as also demonstrated by the control biotubes in this study (Figure 4). Therefore, this study examined the possibility of preparing better biotube vascular grafts using the controlled release of eosin Y.

Eosin is a fluorescent red dye that is used to stain cytoplasm, collagen, and muscle fiber, facilitating their visualization under a microscope.[14] As a result, eosin is most often

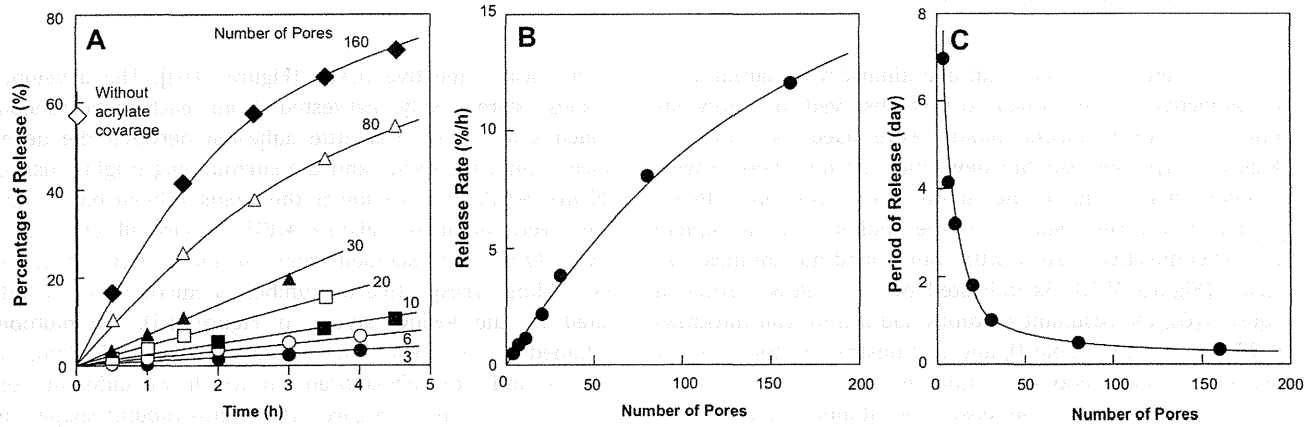

FIGURE 3. A: Release curves of eosin Y from the molds into PBS (100 mL). B: Estimated release rate (%/h) determined from the initial slopes in (A). C: Calculated period of release (days) from the data in (B).

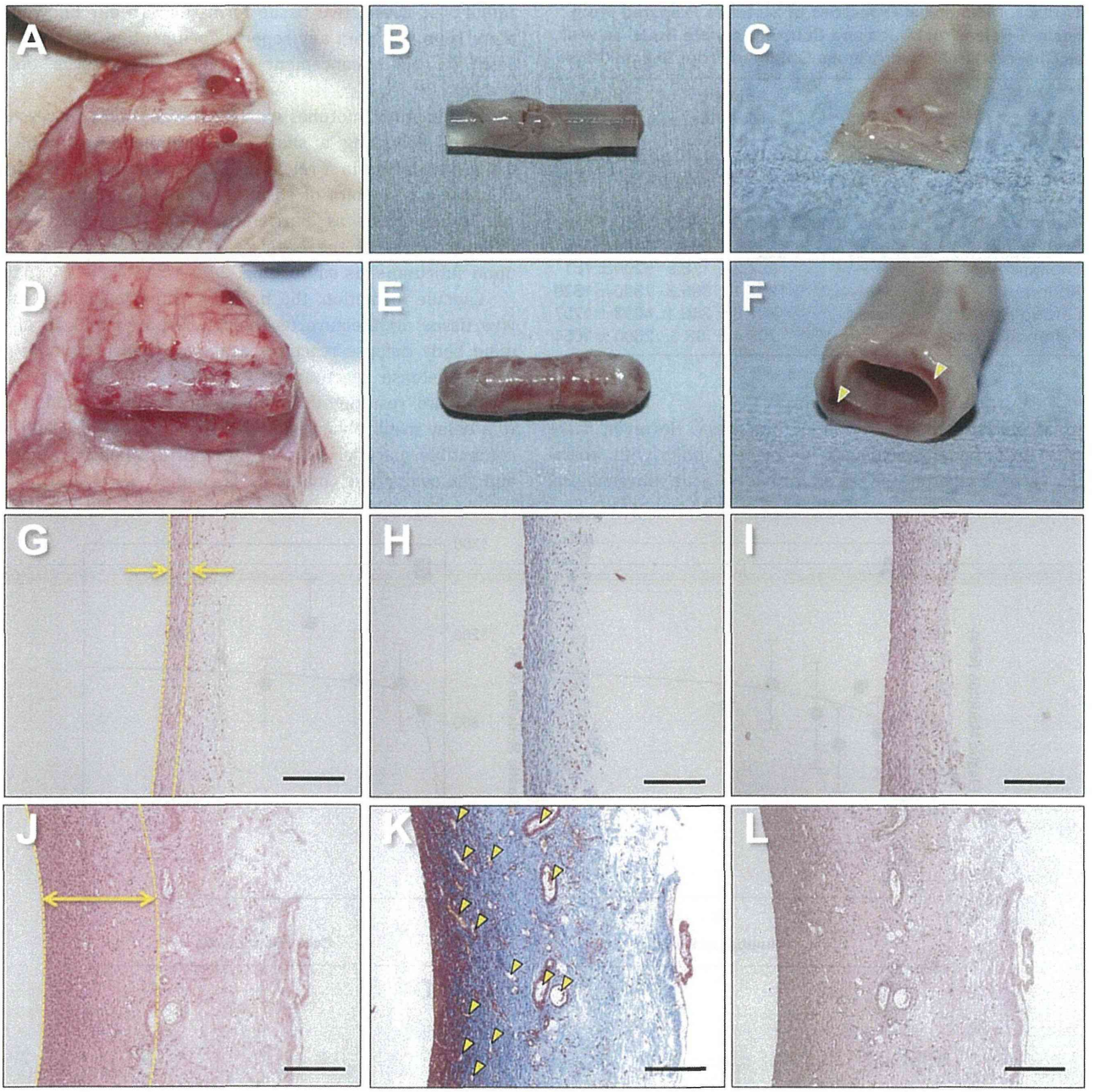

FIGURE 4. A: Macroscopic observation of a biotube formed around the control acrylate mold in the subcutaneous space and the external view of the incomplete biotube with (B) or without (C) the acrylate mold. D: Macroscopic observation of biotube formed around the eosin Y-releasing mold in the subcutaneous space and an external view of the biotube with (E) or without (F) the acrylate mold. Circumferential sections of biotubes prepared from the acrylate molds (G, H, I) and from the eosin Y-releasing molds (J, K, L). Hematoxylin and eosin stained biotube sections (G, J). Masson trichrome stained biotube sections (H, K). Elastica-van Gieson stained biotube sections (I, L). The yellow arrows in G and J shows the layers of the biotubes, which were connected with very fragile mucous membrane-like connective tissues at their outer surfaces. The yellow arrow heads in K indicate capillaries. In all histological photos (G–L), the luminal side is on the left. Bar = 200 μm.

used as a counterstain to hematoxylin, and together, they constitute one of the most commonly used staining techniques in histology. Eosin can also be used as a photo-crosslinkable compound for the preparation of hydrogels because it can generate radicals that form covalent bonds by a proton transfer reaction upon photoirradiaton.[16] Therefore, photo-crosslinkable gelatin, prepared by partial derivatization of eosin Y into gelatin, has been investigated for use in a number of biomedical applications, e.g., as a matrix for drug delivery,[16] a tissue adhesive,[15,17] a post-operative wound dressing, a coating material for implantable medical devices,[18] and as a scaffold material in regenerative medicine.[19] Recently, eosin Y-derivatized gelatins have also been used as coating materials for drug immobilization on molds

TABLE I. Mechanical Properties of Biotubes Prepared From Eosin Y-Releasing Molds and Control Acrylate Rods, as well as Observed in Native Arteries Obtained From Beagle Dogs

Sample	Thickness (μm)	Elastic Modulus (kPa)	Burst Pressure (mmHg)
Eosin Y-releasing Mold	418.2 ± 173.4	956.2 ± 196.5	5850 ± 2383
Acrylate Rod	97.2 ± 22.8	254.5 ± 188.0	1050 ± 446
Aortic Arch	–	499.4 ± 88.8	4550 ± 346
Thoracic Aorta	–	652.2 ± 178.9	5200 ± 751
Abdominal Aorta	–	1267.1 ± 335.3	7350 ± 1820
Carotid Artery	–	787.8 ± 246.1	4013 ± 1297
Pulmonary Artery	–	709.4 ± 93.6	2300 ± 1051

to accelerate the fabrication of biotubes.[9] However, there was little benefit achieved by coating only with eosin-derivatized gelatin; the eosin provided little physiological activity for connective tissue formation. To our knowledge, there have not been any reports documenting the effects of eosin on the enhancement of tissue ingrowth or on its toxicity.

In this study, biotubes with thick walls were successfully prepared following a short, 5-day embedding period by using a novel eosin Y-releasing mold. The agar tubes acted as storage reservoirs of eosin Y and the microporous acrylate tubes acted as barriers for its controlled release, although most of the eosin was released from the mold upon subcutaneous embedding.

Capsule formation, the primary principle involved in *in vivo* tissue architecture technology, is based on one of the main body defense reactions against artificial implants. If a strong defense reaction occurs, excess inflammatory cells accumulate, resulting in inhibition of capsule formation, due to a delay in fibroblast ingrowth. Acrylate, an inert and biocompatible material used in the control molds, is an inert and biocompatible material, is widely used in medical

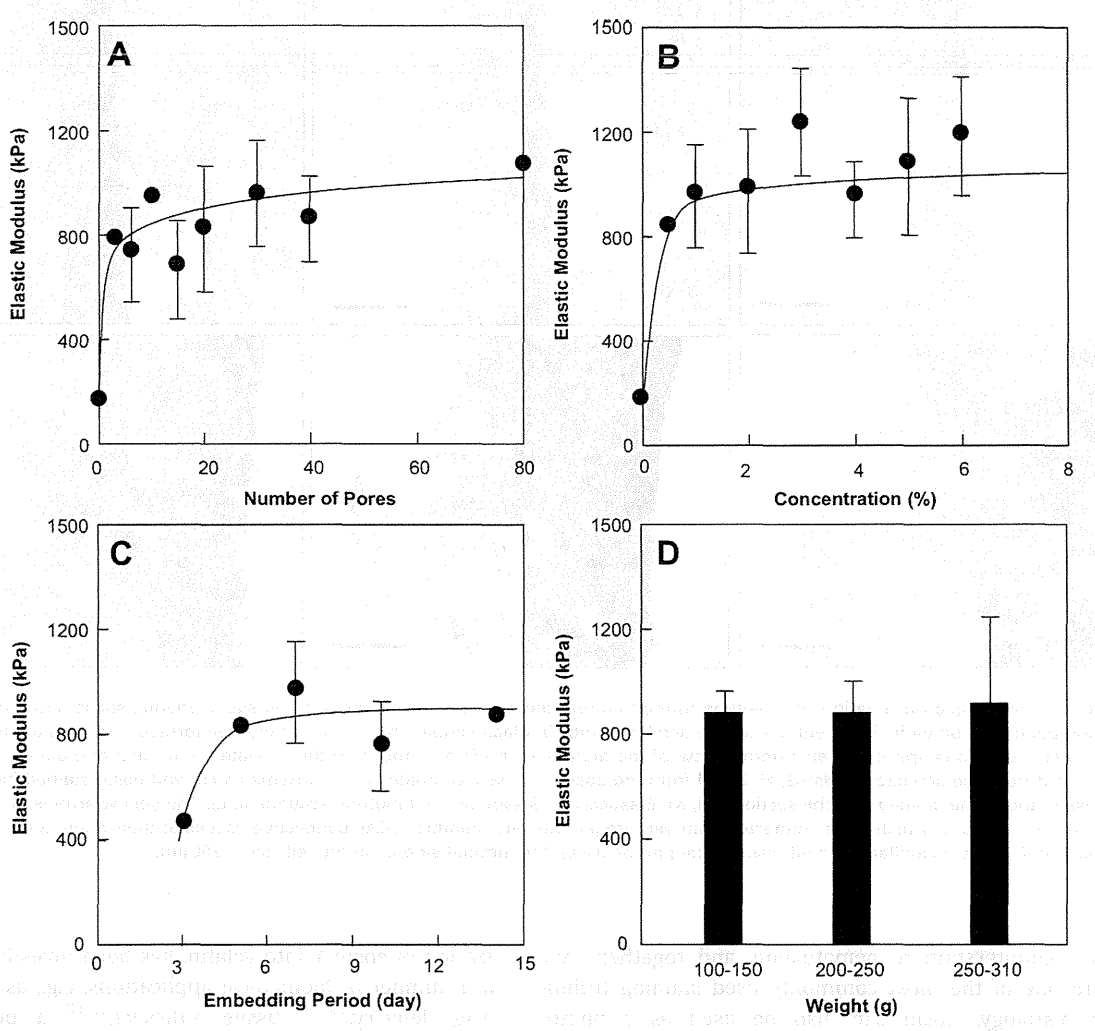

FIGURE 5. Biotubes formed from eosin Y release molds. The relationships between elastic modulus and number of pores (A), the concentration of eosin Y in the molds (B), the length of the embedding period (C), and the weight of rats (D). Preparation conditions in (A): 1% w/v concentration of eosin Y, and an embedding period of 7 days; in (B): the number of micropores = 30, with an embedding period of 7 days; in (C): the number of micropores = 30, with a 1% (w/v) concentration of eosin Y; in (D): the number of micropores = 30, with a 1% (w/v) concentration of eosin Y, and an embedding period of 7 days.

devices and does not allow sufficient capsule formation with a 1-week embedding period. The release of eosin Y, however, significantly enhanced capsule formation. Even though there is a little report about physiological activity of eosin Y, an appropriate host defense reaction was stimulated by the release of eosin Y, resulting in enhanced biotube formation. Interestingly, neither the number of pores in the acrylate nor the concentration of eosin Y had significant effects on the robust formation of biotubes. This suggested that a little stimulation by eosin Y would control connective tissue formation and further suggested that the releasing molds reported in this study might be used in other applications without toxicity.

One of the most effective methods to activate angiogenesis is the introduction of bioactive substances, such as cytokines, vascular endothelial growth factor (VEGF),[20,21] and basic fibroblast growth factor (bFGF).[22,23] The slow release of VEGF has been reported to promote angiogenesis and is effective in neovascularization therapy for peripheral, arterial, and cardiac ischemia. In a preliminary study, the slow release of VEGF from the mold surface promoted neovascularization in biotube tissue (data not shown). Furthermore, impregnation of VEGF into polyurethane grafts enhanced the ingrowth of transanastomatic tissues and transluminal capillaries.[24] Therefore, other compounds, such as VEGF, bFGF, or nicotine, are expected to function in a similar physiological manner when released from these microporous molds and may allow further enhancement of biotube formation.

Capillary formation is one of the most important requirements for the construction of three-dimensional, thick, and functional tissues in tissue engineering, as the diffusional supply of oxygen can only support a tissue thickness of less than 200 μm. Eosin Y stimulation also induced the significant formation of matured capillaries, composed of both endothelial cells and smooth muscle cells. These neovessels also supported the increased thickness of the biotube tissues. Natural, strong antithrombogenic activity is provided by the complete endothelialization of the luminal surface and is highly desirable. However, the preparation of an endothelialized-biotube surface in an *in vivo* reactor is extremely difficult and the preparation of such a surface *in vitro* requires complex cell management and processing. Therefore, wall structures that attain complete endothelialization at an early stage of the implantation are desirable. Furthermore, rich angiogenesis, including the recruitment of large numbers of endothelial cells, in the biotube walls was hypothesized to promote endothelialization of the luminal surface. In other words, upon contact with the blood flow after implantation, capillary migration from the wall to the luminal surface could be induced in order to supply the endothelial cells.

In this study, significant cellular migration to the surface of the acrylate rods with concomitant angiogenesis was promoted by eosin Y release. The tissue that formed on the surface of the structure was primarily colonized by fibroblasts. To our knowledge, this is the first report describing the acceleration of tissue formation triggered by eosin Y. However, it was considered that eosin Y itself had a very little activity for tissue formation or anigiogenesis. In encapsulation process of this study, continuous weak stimulation by eosin Y was effective. Degree of stimulation might be important in enhancement of the process. Too much stimulation would induce inflammation reaction. Therefore, other inert chemicals even with a little physiological activity for tissue formation or anigiogenesis could enhance the encapsulation. Biotubes with remarkably thick walls and an appropriate rigidity were formed within the short, 5-day embedding period. Since efficient nutrition was maintained as a results of the rich angiogenesis throughout the wall, the newly developed tissue could survive even within the thick surrounding tissues. We are currently devising animal experiments to evaluate the *in vivo* performance of these newly developed biotubes.

CONCLUSIONS

The application of the newly developed eosin Y-releasing mold brought about accelerated fabrication of thick-walled biotubes with robust angiogenesis that may be used as large-caliber vascular grafts. The biotubes exhibited mechanical properties, including sufficient rigidity to maintain patency for easy anastomosis and a high elastic modulus for withstanding blood pressure changes, which were suitable for such applications.

ACKNOWLEDGMENTS

The authors thank Ms. Manami Sone for her technical support in this study.

REFERENCES

1. Hibino N, McGillicuddy E, Matsumura G, Ichihara T, Naito Y, Breuer C, Shin'oka T. Late-term results of tissue-engineered vascular grafts in humans. J Thorac Cardiovasc Surg 2010;139: 431–436.
2. Yokota T, Ichikawa H, Matsumiya G, Kuratani T, Sakaguchi T, Iwai S, Shirakawa Y, Torikai K, Saito A, Uchimura E, Kawaguchi N, Matsuura N, Sawa Y. In situ tissue regeneration using a novel tissue-engineered, small-caliber vascular graft without cell seeding. J Thorac Cardiovasc Surg 2008;136:900–907.
3. Iwasaki K, Kojima K, Kodama S, Paz AC, Chambers M, Umezu M, Vacanti CA. Bioengineered three-layered robust and elastic artery using hemodynamically-equivalent pulsatile bioreactor. Circulation 2008;118:S52–S57.
4. Quint C, Kondo Y, Manson RJ, Lawson JH, Dardik A, Niklason LE. Decellularized tissue-engineered blood vessel as an arterial conduit. Proc Natl Acad Sci USA 2011;108:9214–9219.
5. Helne J, Schmiedl A, Cebotari S, Karck M, Mertsching H, Haverich A, Kallenbach K. Tissue engineering human small-caliber autologous vessels using a xenogenous decellularized connective tissue matrix approach: Preclinical comparative biomechanical studies. Artif Organs 2011;35:930–940.
6. Huang H, Zhou YM, Ishibashi-Ueda H, Takamizawa K, Ando J, Kanda K, Yaku H, Nakayama Y. In vitro maturation of "biotube" vascular grafts induced by a 2-day pulsatile flow loading. J Biomed Mater Res B Appl Biomater 2009;91:320–328.
7. Nakayama Y, Ishibashi-Ueda H, Takamizawa K. In vivo-tissue engineered small-caliber vascular graft prosthesis consisting of autologous tissue (biotube). Cell Transplant 2004;13:439–449.
8. Sakai O, Kanda K, Ishibashi-Ueda H, Takamizawa K, Ametani A, Yaku H, Nakayama Y. Development of the wing-attached rod for acceleration of "Biotube" vascular grafts fabrication in vivo. J Biomed Mater Res B Appl Biomater 2009;90:412–420.

9. Sakai O, Kanda K, Takamizawa K, Sato T, Yaku H, Nakayama Y. Faster and stronger vascular "Biotube" graft fabrication in vivo using a novel nicotine-containing mold. J Biomed Mater Res B Appl Biomater 2009;90:412–420.
10. Heeschen C, Weis M, Cooke JP. Nicotin promotes arteriogenesis. J Am Coll Cardiol 2003;41:489–496.
11. Yamanami M, Yamamoto A, Iida H, Watanabe T, Kanda K, Yaku H, Nakayama Y. 3-Tesla magnetic resonance angiographic assessment of a tissue-engineered small-caliber vascular graft implantation in a rat. J Biomed Mater Res B Appl Biomater 2010;92: 156–160.
12. Watanabe T, Kanda K, Yamanami M, Ishibashi-Ueda H, Yaku H, Nakayama Y. Long-term animal implantation study of biotube-autologous small-caliber vascular graft fabricated by in-body tissue architecture. J Biomed Mater Res B Appl Biomater 2011;98: 120–126.
13. Watanabe T, Kanda K, Ishibashi-Ueda H, Yaku H, Nakayama Y. Autologous small-caliber "biotube" vascular grafts with argatroban loading: A histological examination after implantation to rabbits. J Biomed Mater Res B Appl Biomater 2010;92:236–242.
14. Jocelyn H. Bruce-Gregorios, MD.: Histopathologic Techniques, JMC Press Inc., Quezon City, Philippines, 1974.
15. Nakayama Y, Matsuda T. Photocurable surgical tissue adhesive glues composed of photoreactive gelatin and poly(ethylene glycol) diacrylate. J Biomed Mater Res 1999;48:511–521.
16. Okino H, Nakayama Y, Tanaka M, Matsuda T. In situ hydrogelation of photocurable gelation and drug release. J Biomed Mater Res 2002;59:233–245.
17. Nakayama Y, Matsuda T. Newly designed hemostatic technology based on photocurable gelatin. ASAIO J 1995;41:M374–M378.
18. Nakayama Y, Ji-Youn K, Nishi S, Ueno H, Matsuda T. Development of high-performance stent: gelatinous photogel-coated stent that permits drug delivery and gene transfer. J Biomed Mater Res 2001;57:559–566.
19. Fukaya C, Nakayama Y, Murayama Y, Omata S, Ishikawa A, Hosaka Y, Nakayama Y. Improvement of hydrogelation ability and handling of photocurable gelatin-based crosslinking materials. J Biomed Mater Res B Appl Biomater 2009;91:329–336.
20. Witzenbichler B, Asahara T, Murohara T, Silver M, Spyridopoulos I, Magner M, Principe N, Kearney M, Hu JS, Isner JM. Vascular endothelial growth factor-C (VEGF-C/VEGF-2) promotes anigiogenesis in the setting of tissue ischemia. Am J Pathol 1998;153:381–394.
21. Silvestre JS, Tamarat R, Ebrahimian TG, Le-Roux A, Clergue M, Emmanuel F, Duriez M, Schwartz B, Branellec D, Lévy BI. Vascular endothelial growth factor-B promotes in vivo angiogenesis. Circ Res 2003;93:114–123.
22. Hosseinkhani H, Hosseinkhani M, Khademhosseini A, Kobayashi H, Tabata Y. Enhanced angiogenesis through controlled release of basic fibroblast growth factor from peptide amphiphile for tissue regeneration. Biomaterials 2006;27:5836–5844.
23. Schweigerer L, Neufeld G, Friedman J, Abraham JA, Fiddes JC, Gospodarowicz D. Capillary endothelial cells express basic fibroblast growth factor, a mitogen that promotes their own growth. Nature 1987;325:257–259.
24. Masuda S, Doi K, Satoh S, Oka T, Matsuda T. Vascular endothelial growth factor enhances vascularization in microporous small caliber polyurethane grafts. ASAIO J 1997;43:M530–M534.

JOURNAL OF TISSUE ENGINEERING AND REGENERATIVE MEDICINE
J Tissue Eng Regen Med (2013)
Published online in Wiley Online Library (wileyonlinelibrary.com) **DOI:** 10.1002/term.1859

RESEARCH ARTICLE

In-body tissue-engineered collagenous connective tissue membranes (BIOSHEETs) for potential corneal stromal substitution

Naoaki Takiyama[1], Takeshi Mizuno[1,2], Ryosuke Iwai[2], Masami Uechi[1,2] and Yasuhide Nakayama[2]*
[1]*Department of Veterinary Medicine, College of Bioresource Sciences, Nihon University, Kanagawa, Japan*
[2]*Division of Medical Engineering and Materials, National Cerebral and Cardiovascular Centre Research Institute, Osaka, Japan*

Abstract

There is a severe shortage of donor cornea for transplantation in many countries. Collagenous connective tissue membranes, named BIOSHEETs, grown *in vivo* were successfully implanted in rabbit corneal stroma for *in vivo* evaluation of their suitability as a corneal stromal substitute to solve this global donor shortage. BIOSHEETs were prepared by embedding silicone moulds into dorsal subcutaneous pouches in rabbits for 1 month and stored in glycerol. After re-swelling in saline and trephining, disk-shaped BIOSHEETs (4 mm diameter) were allogeneically implanted into stromal pockets prepared in the right cornea of seven rabbits. Clinical tests for corneal thickness and transparency, and tissue analyses were performed. Because the BIOSHEETs (thickness, 131 ± 14 μm) obtained were opaque immediately after implantation, the transparency of the cornea decreased. The total thickness of the BIOSHEET-implanted cornea increased from 364 ± 21.0 μm to 726 ± 131 μm. After 4 weeks' implantation, the thickness of the cornea stabilized (493 ± 80 μm at 4 weeks and 447 ± 46 μm at 8 weeks). The transparency of the cornea increased progressively with time of implantation. The random orientation of collagen fibrils in the original BIOSHEETs tended to be homogeneous, similar to that of the native stroma. No inflammatory cells accumulated and fibroblast-like cells infiltrated the implant. The BIOSHEETs showed high biocompatibility with stromal tissues; however, further studies are needed to test its functional aspects. Although this research is only intended as a proof of concept, BIOSHEETs may be considered a feasible corneal stromal replacement, especially for treating visual impairment caused by stromal haze.

Received 28 March 2013; Revised 7 September 2013; Accepted 10 November 2013

Keywords **biocompatibility; connective tissue; cornea; implantation; tissue engineering**

1. Introduction

The cornea is the transparent outer window to the eye and is one of the major refractive elements of the eye. The corneal stroma, which is a collagenous hydrogel with lesser amounts of glycosaminoglycans (proteoglycans that contains keratocytes) is sandwiched by non-keratinizing epithelium and inner single-layered endothelium. The corneal stroma comprises 90% of the thickness of the cornea and consists of regularly packed collagen fibrils arranged as orthogonal layers or lamellae. Approximately 70% of the dry weight of the corneal stroma is composed of collagen type I. The collagen fibrils of this tissue are regularly spaced, similar in diameter and run parallel to one another within lamellae. The transparency of the corneal stroma is attributed to the unique tight packing and uniform diameter of the collagen fibrils, which minimizes light scattering (Robert *et al.*, 2001; Knupp *et al.*, 2009; Hassell and Birk, 2010).

Corneal disorders that disrupt the uniformity of the stromal structure result in a loss of corneal transparency. Corneal disease is a major cause of blindness or severely impaired vision and affects more than 10 million people worldwide. In some parts of Africa and Asia the

* *Correspondence to: Yasuhide Nakayama, Division of Medical Engineering and Materials, National Cerebral and Cardiovascular Centre Research Institute, 5-7-1 Fujishirodai, Suita, Osaka 565–8565, Japan. E-mail: nakayama@ncvc.go.jp*

incidence of childhood cornea-related visual loss is 20 times higher than that in industrialized countries (Schwartz *et al.*, 1997; Whitcher *et al.*, 2001, 2002). Blindness caused by corneal disease is usually permanent. The only widely accepted treatment for corneal blindness is corneal transplantation.

However, there is a severe shortage of acceptable corneal tissue for transplantation, especially with the increase in the aging population and incidence of transmissible disease. Corneal transplantation has many limitations, including a lack of eye banking infrastructure and excessive cost, particularly in the Third World and developing countries (Feilmeier *et al.*, 2010). In addition, in so-called 'high-risk cases' where the recipient corneal bed is inflamed and/or neo-vascularized, the prognosis is poor and the graft failure rate is high (Streilein *et al.*, 1999; Williams and Coster, 2007; Chong and Dana, 2008).

Many groups have attempted to construct corneal substitutes. Various compounds have been used in corneal research, including synthetic materials such as silicone rubber, polymethylmethacrylate (PMMA), poly (2-hydroxyethyl methacrylate) or naturally occurring polymers such as collagen and hyaluronic acid, collagen-glycosaminogycan-chitosan and silk fibroin (Crawford *et al.*, 1993; Doane *et al.*, 1996; Lee *et al.*, 1996; Vijayasekaran *et al.*, 1997; Chen *et al.*, 2005; Builles *et al.*, 2007; Bray *et al.*, 2011). However, biological integration with the surrounding recipient tissue is still a major problem, and restoration of sensory or physiological corneal function has not been achieved. Alternatively, many groups have attempted to develop tissue-engineered corneal equivalents (Liu *et al.*, 2007; Fagerholm *et al.*, 2009, 2010; Merrett *et al.*, 2009; Duncan *et al.*, 2010; Tanaka *et al.*, 2011; Xiao *et al.*, 2011; Yoeruek *et al.*, 2011). An ideal scaffold for a tissue-engineered corneal equivalent should be biocompatible, non-immunogenic, non-mutagenic, sufficiently strong to withstand surgical procedures and optically clear (Feinberg, 2012). Therefore, the primary goal of this study was to prepare unique collagenous membranes (hereafter termed BIOSHEETs) for corneal stroma substitution by in-body tissue engineering (Nakayama *et al.*, 2004; Watanabe *et al.*, 2011; Hayashida *et al.*, 2007; Yamanami *et al.*, 2010). In this study, BIOSHEETs were prepared using in-body tissue engineering and transplanted into rabbit corneal stroma. The aim was to evaluate the biocompatibility, the transparency and the possibility of the BIOSHEETs as a potential corneal stroma substitution material *in vivo*.

2. Materials and methods

2.1. Animal studies

Studies were performed in accordance with the National Institutes of Health (NIH) guidelines for the care and use of laboratory animals' (National Institutes of Health 1996) and the Association for Research in Vision and Ophthalmology (ARVO) statement for the use of animals in ophthalmic and vision research under a protocol approved by the National Cerebral and Cardiovascular Center Research Institute Committee (No. 12002).

2.2. BIOSHEET preparation protocol

The mould for BIOSHEETs (Figure 1a) was prepared by terminal adhesion of silicone tubes (60 mm long, 20 mm diameter, 2 mm thick). Six Japanese white rabbits (2.7–3.0 kg) were given general anesthesia using a mixture of ketamine (50 mg/kg Ketalar; Daiichi Sankyo, Tokyo, Japan) and xylazine (5 mg/kg Selactar; Bayer Health Care, Tokyo, Japan) and maintained by bolus intramuscular injection of a quarter of the initial dose. A 5 cm incision was made at dorsal skin between last rib and ilium, and two moulds were placed into each subcutaneous pouch (Figure 1b), each incision was then sutured with 4–0 nylon (Figure 1c). The rabbits received 5 mg/kg systemic enrofloxacin (Baytril injectable; Bayer, Tokyo, Japan) for 1 week. After complete encapsulation of the moulds by connective tissue (i.e. 1 month after implantation) the implants were harvested (Figure 1d). The membranous tissue that formed as a BIOSHEET around the mould was obtained by trimming to remove fragile and redundant tissue adhered to the BIOSHEET tissue (Figure 1e). The BIOSHEETs were preserved by soaking in sterile pure glycerol (Wako Pure Chemical, Osaka, Japan), which is used clinically to preserve donor corneas for corneal transplantation in the developing world, at 4 °C for 1 week. Before implantation, BIOSHEETs were submerged in sterile physiological saline to allow irrigation for 10 min (Figure 1f).

2.3. BIOSHEET implantation procedure

The BIOSHEETs were implanted as an allogenic stromal substitute into the right cornea of seven Japanese white rabbits (2.8–3.0 kg). Rabbits were anesthetized with medetomidine (0.1 mg/kg Dorbene; Kyoritsu Seiyaku, Tokyo, Japan), butorphanol (0.2 mg/kg Vetorfal; Meiji Seika Pharma, Tokyo, Japan) and ketamine (25 mg/kg Ketalar; Daiichi Sankyo). In addition, oxybuprocaine hydrochloride (Benoxil ophthalmic solution 0.4%; Santen Seiyaku, Osaka, Japan) was given twice before surgery for induction of local anaesthesia. A 6-mm long incision with a depth approximately half that of the cornea was made at the dorsal limbus, and a stromal pocket was created using a scleral knife. A BIOSHEET was trephined to provide disks with a diameter of 4 mm (Figure 1h) and implanted into the pocket (Figure 1i). One of the six BIOSHEETs was used for transplantation to eliminate the potential confounding factor of biocompatibility. Control cornea received sham surgery